

ANALYSIS OF DYNAMIC CHARACTERISTICS OF A SEALED ENDS SQUEEZE FILM DAMPER CONSIDERING THE FLUID INERTIA FORCE

HAI LUN ZHOU, YANG GUANG CANG, YU QI ZHANG, CHAO GUO

School of Aero-engine, Shenyang Aerospace University, Shenyang, China, and Liaoning Key Laboratory of Advanced Measurement and Test Technology for Aircraft Propulsion System, School of Economics and Management,

Tongji University, Shanghai, China

Corresponding author Chao Guo, e-mail: gczq@163.com

In order to effectively calculate dynamic characteristics of a sealed ends squeeze film damper (SFD) under the influence of the inertial force, a computational fluid dynamics model of the sealed ends SFD is established. The fluid inertia coefficient of SFD is investigated by using an energy approximation method. Both the theoretical calculation and numerical simulation are conducted to analyze the effects of eccentricity ratio and whirling frequency on stiffness and damping. In this research, the oil film inertia force of the sealed ends SFD is solved by using long bearing approximation (LBA) theory, which provides guidance for the design and application of the sealed ends SFD.

Keywords: squeeze film damper, fluid inertia, computational fluid dynamics, damping, stiffness

1. Introduction

Squeeze film dampers (SFDs) suppress vibration and enhance stability of rotating machines (Miyachi *et al.*, 1979). In the LBA to Reynolds equation, which is justified if a damper is long in the axial direction, the flow in the damper is circumferential, and thus the circumferential pressure gradient is much larger than the axial pressure gradient. In practice, if the damper is tightly sealed, the flow is circumferential even if the dampers are physically short. In this case, the LBA would describe the conditions better than the short bearing approximation (SBA) (El-Shafei and Crandall, 1991). SFDs with sealed ends absorb more vibration than open ends SFDs when passing critical speeds under the same operation condition as sealed SFDs produce more damping (San Andrés and Seshagiri, 2013). But current and related investigations are not sufficient in that matter.

Establishing accurate mathematical functions is difficult as fluid motion inside the oil film clearance is complicated, so logical simplifications and assumptions are compulsive. In classical lubrication theory, fluid inertia is neglected and the Reynolds equation governing SFDs is obtained (Szeri, 1980). However, past examinations have revealed that film forces calculated by theoretical functions do not correspond with the results obtained from experiments due to neglect of fluid inertia, and the error could even go up to 60%. The fluid inertia should be taken into consideration when the Reynolds number is larger than 1.

Researchers paid attention to the effects of fluid inertia many years ago. Kuzma (1968) demonstrated that the fluid inertia produced a significant squeeze film effect, and the theoretical model considering the fluid inertia corresponded with experimental results well. Chen *et al.* (2021) investigated dynamics of a rotor system supported on SFD considering the fluid inertia. Numerical integration was employed to calculate the pressure and oil film force. The results showed that oil film pressure was sensitive to fluid inertia when the journal eccentricity ratio

was large. The radial force decreased while the tangential force increased. The fluid inertia suppressed the resonance amplitude under high rotating speed and large eccentricity. San Andrés investigated the effect of fluid inertia on rotor dynamics supported on an SFD and found that increasing fluid inertia reduced the occurrence of bistable operation and jump phenomena (San Andrés and Vance, 1988). Hamzehlouia and Behdinan (Hamzehlouia and Behdinan, 2016) did numerical analysis towards a finite length SFD considering the unstable state inertia term, and compared the results with the existing SFD model. The comparison showed that the fluid inertia produced a significant effect on the oil film pressure and force even at small Reynolds numbers.

With the development of computers, computational fluid dynamics (CFD) software has been employed to do simulations on SFDs. The CFD software make complex geometric model flow analysis available (Guo *et al.*, 2005). Lee *et al.* (2017) investigated the effect of oil supply groove and sealed piston ring on the oil film at a small clearance using CFD software. The results showed that the oil film pressure decreased as oil supply depth, piston ring radial clearance and axial clearance increased, and the radial and tangential forces decreased accordingly. Dousti *et al.* (2016) addressed the oil film pressure distribution and oil film force changing under different groove depths and rotating speeds through CFX software. The results indicated that considerable pressure was generated in a sealed groove, and the pressure changed along the circumferential direction rather than the axial one. Zhou *et al.* (2020a,b) calculated SFD dynamic characteristics with SBA, which provide more ideas for the open ends SFD design.

Szeri *et al.* (1982) added an acceleration term and pointed out that oil film reaction forces were generated by both viscous and inertial forces. El-Shafei (1991) used momentum and energy approximation to analyze the inertial term independently of the viscous term. The inertial term was determined by the Lagrange equation and Reynolds transport law.

Through the above research, it is found that the effect of oil film fluid inertia on SFD dynamic characteristic is mostly based on a short open ends SFD, but there are few theoretical studies on the LBA considering the oil film inertia force and numerical simulation of dynamic characteristics of the sealed ends SFD. This paper investigates the fluid inertia effect using the energy approximation method (Crandall and El-Shafei, 1993) and derives stiffness and damping coefficients with the LBA. The numerical simulation is conducted on CFX to verify the derived functions. Based on the functions and simulations, the effects of frequency and eccentricity ratio on SFD dynamic characteristics are analyzed.

2. Long bearing approximation theoretical analysis

2.1. Analysis of the long bearing approximation SFD viscosity term

The LBA theory assumes that if the axial length is long enough or there are seals at both ends, the oil film pressure gradient along circumferential direction is much larger than that along the axial one, and the changes in the circumferential direction are much larger than in the axial direction. In order to study dynamic characteristics of the sealed ends SFD, the LBA theoretical analysis was carried out.

The structure of an SFD is usually simplified for deducing dynamic characteristics formula of the SFD and the corresponding coordinate system is established, as shown in Fig. 1a. Taking the middle line of the central groove as the reference line, the left or right part of the structure is extracted, which is shown in Fig. 1b, where O_b is the origin of the SFD coordinate system in the center of the SFD housing, O_j is the center of the journal, h is thickness of the oil film, θ measured from the positive r -axis of the rotating coordinate system (r, t, z) , ϕ is the static coordinate system (x, y, z) and from the positive x axis. The measured angle is $\theta = \phi - \psi$. For stable circular precession $\psi = \omega t$, where ω is the journal rotation speed, e is the dynamic

eccentricity of the SFD journal, X is the circumferential direction, Y is the normal direction, z is the axis direction of the journal, R is radius of the SFD journal, L is the SFD axial length.

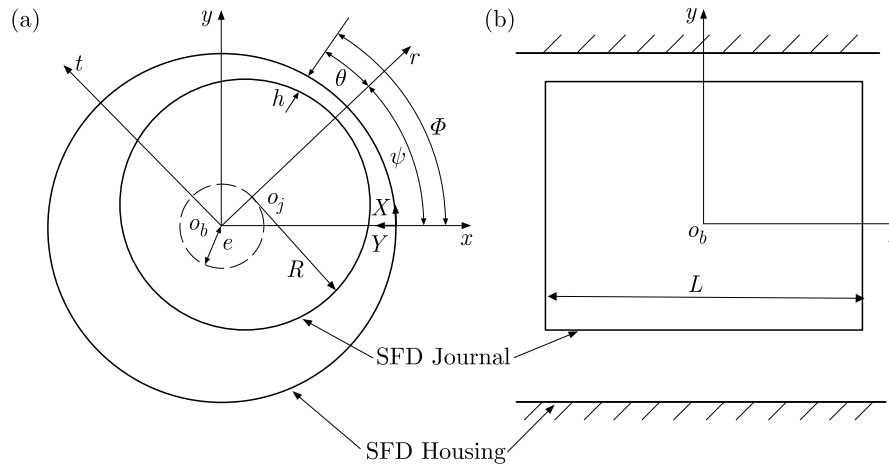


Fig. 1. SFD coordinate system

Since the NS equation is a nonlinear partial differential equation, it cannot be directly used to solve the SFD oil film pressure. The Reynolds equation is simplified from the NS equation with several assumptions in the case of low viscosity flow. The pressure distribution and oil film force of the SFD can be obtained with appropriate boundary conditions. The Reynolds equation is as follows

$$\frac{1}{R^2} \frac{\partial}{\partial \theta} \left(\frac{h^3}{\mu} \frac{\partial P}{\partial \theta} \right) + \frac{\partial}{\partial z} \left(\frac{h^3}{\mu} \frac{\partial P}{\partial z} \right) = 6(\omega_j - 2\dot{\psi}) \frac{\partial h}{\partial \theta} + 12 \frac{de}{dt} \cos \theta \quad (2.1)$$

Since the journal of the damper does not rotate and the housing is fixed, precession will only occur due to an unbalanced excitation, so the journal rotation speed ω_j is 0.

According to the geometric relationship shown in Fig. 1, the film thickness h at any given location is given by

$$h = c(1 - \varepsilon \cos \theta) \quad (2.2)$$

where c is the clearance, ε is the eccentricity ratio of the journal, $\varepsilon = e/c$.

In a simplified analysis, it is considered that the oil film pressure does not change along the thickness of the oil film, and the damper journal only performs stable circular motion. Neither the damper housing nor the journal rotates, the SFD Reynolds equation is obtained as

$$\frac{1}{R^2} \frac{\partial}{\partial \theta} \left(h^3 \frac{\partial P}{\partial \theta} \right) + \frac{\partial}{\partial z} \left(h^3 \frac{\partial P}{\partial z} \right) = -12\dot{\psi}\mu \frac{\partial h}{\partial \theta} \quad (2.3)$$

In LBA theory, the pressure gradient along axial direction is negligible comparing with the circumferential direction, so $\partial P/\partial z$ term is omitted and the following equation is obtained

$$\frac{1}{R^2} \frac{\partial}{\partial \theta} \left(h^3 \frac{\partial P}{\partial \theta} \right) = -12\dot{\psi}\mu \frac{\partial h}{\partial \theta} \quad (2.4)$$

where μ is viscosity of the oil, R is radius of the journal, P is pressure, \dot{e} and $e\dot{\psi}$ are the radial and tangential velocity of the journal, respectively.

Integrating twice with π -film boundary conditions (Booker, 1965), the oil film pressure is

$$P = \frac{6\mu R^2}{c^3} \left\{ \left[\frac{1}{\varepsilon(1 - \varepsilon \cos \theta)^2} - \frac{1}{\varepsilon(1 + \varepsilon)^2} \right] \dot{e} + \left[\frac{2 \sin \theta (2 - \varepsilon \cos \theta)}{(2 + \varepsilon^2)(1 - \varepsilon \cos \theta)^2} \right] e\dot{\psi} \right\} \quad (2.5)$$

Area-integrating the pressure and decomposing it tangentially and radially

$$\begin{aligned} F_{rc} &= -\frac{\mu R^3 L}{c^3} \frac{6\pi}{(1-\varepsilon^2)^{\frac{3}{2}}} \dot{e} - \frac{\mu R^3 L}{c^3} \frac{24\varepsilon}{(2+\varepsilon^2)(1-\varepsilon^2)} e\dot{\psi} \\ F_{tc} &= -\frac{\mu R^3 L}{c^3} \frac{24}{(1+\varepsilon^2)(1-\varepsilon^2)} \dot{e} - \frac{\mu R^3 L}{c^3} \frac{12\pi}{(2+\varepsilon^2)(1-\varepsilon^2)^{\frac{1}{2}}} e\dot{\psi} \end{aligned} \quad (2.6)$$

The radial and tangential viscosity damping forces acting on the journal F_{rc} and F_{tc} are determined, respectively.

2.2. Analysis of the SFD inertia term of long bearing approximation

Based on the assumption that the velocity distribution with inertia is the same as that of inertialess fluids, the fluid inertial forces in the long damper are obtained by using the energy approximation method (El-Shafei and Crandall, 1991). For a long damper, the circumferential velocity is solved based on the Reynolds equation as

$$u = \frac{6R}{h} \left(\frac{Y}{h} - \frac{Y^2}{h^2} \right) \left[\dot{e} \sin \theta - e\dot{\psi} \cos \theta + \frac{3\varepsilon}{2+\varepsilon^2} e\dot{\psi} \right] \quad (2.7)$$

At a particular time t , it is convenient to establish a control volume consistent with the fluid mass boundary. Over some time, the control volume remains fixed in space, while the fixed unit of fluid mass changes its shape: the extrusion film becomes thinner and the suction film thickens. Some fixed characteristic fluid near the end of the extrusion film is expelled from the control volume, and some new fluid not belonging to the fixed characteristic mass is sucked into the control volume at the end of the extrusion film. The dynamic coefficient of the fluid inside the damper is

$$T^* = \frac{1}{2} \int_{\theta_2}^{\theta_1} \int_0^h \int_{-L/2}^{L/2} \rho u^2 R d\theta dY dZ \quad (2.8)$$

When the damper journal is in the steady state circular precession, $\ddot{\psi} = \ddot{e} = \dot{e} = 0$. The dynamic coefficient of the fluid inside the damper can be calculated

$$T^* = \frac{1}{2} \frac{12\rho R^3 L}{10c} \left[\left(\frac{3\varepsilon}{2+\varepsilon^2} \right)^2 \frac{\pi}{(1-\varepsilon^2)^{\frac{1}{2}}} - \frac{6}{2+\varepsilon^2} \left(\frac{\pi}{(1-\varepsilon^2)^{\frac{1}{2}}} - \pi \right) + \frac{1}{\varepsilon^2} \left(\frac{\pi}{(1-\varepsilon^2)^{\frac{1}{2}}} - \pi \right) \right] (e\dot{\psi})^2 \quad (2.9)$$

The inertia forces in the damper can be obtained by Lagrange's equations. The radial and tangential inertial forces obtained by combining the Reynolds transport theorem with the Lagrange equation are

$$F_{ir} = F_{ri} + R_{ri} \quad F_{it} = F_{ti} + R_{ti} \quad (2.10)$$

where F_{ir} is the radial inertial force, F_{it} is the tangential inertial force, R_{ri} and R_{ti} are inertial forces due to the flux of fluid particles across the control surface along the radial and tangential directions, respectively. F_{ri} and F_{ti} obtained by the Lagrange equation are given as follows

$$F_{ri} = -\frac{d}{dt} \left(\frac{\partial T^*}{\partial \dot{e}} \right) + \frac{\partial T^*}{\partial e} \quad F_{ti} = -\frac{1}{e} \frac{d}{dt} \left(\frac{\partial T^*}{\partial \dot{\psi}} \right) + \frac{1}{e} \frac{\partial T^*}{\partial \psi} \quad (2.11)$$

Substituting (2.9) into (2.11), we get

$$F_{ri} = \frac{\partial T^*}{\partial e} = \frac{\partial T^*}{c\partial \varepsilon} = \frac{12\rho R^3 L \pi}{10c(\varepsilon^2 + 2)^2} \left[12 - 2 \frac{(10 - \varepsilon^2)(1 - \varepsilon^2)^{\frac{1}{2}}}{\varepsilon^2 + 2} \right] e(\dot{\psi})^2 \tag{2.12}$$

$$F_{ti} = \frac{1}{e} \frac{\partial T^*}{\partial \psi} = -\frac{1}{e} \frac{12\rho R^3 L}{10c} \left[\frac{\varepsilon(8 + \varepsilon^2)}{(\varepsilon^2 + 2)^2} \right] (e\dot{\psi})^2$$

Since the π -film theory and motion of the SFD journal are mainly studied, the flux terms R_{ri} and R_{ti} are simplified and integrated

$$R_{ri} = 0 \tag{2.13}$$

and

$$R_{ti} = e(\dot{\psi})^2 \frac{\rho R^3 L}{c} \left\{ \underbrace{\left[-\frac{27}{35} \varepsilon \frac{\left(\frac{3\varepsilon}{2+\varepsilon^2} + 1\right)^3}{(1+\varepsilon)^2} + \frac{3}{5} \frac{\left(\frac{3\varepsilon}{2+\varepsilon^2} + 1\right)^2}{1+\varepsilon} \right]}_{\mathcal{A}_1} \right. \tag{2.14}$$

$$\left. + \underbrace{\left[\frac{27}{35} \varepsilon \frac{\left(\frac{3\varepsilon}{2+\varepsilon^2} - 1\right)^3}{(1-\varepsilon)^2} - \frac{3}{5} \frac{\left(\frac{3\varepsilon}{2+\varepsilon^2} - 1\right)^2}{1-\varepsilon} \right]}_{\mathcal{A}_2} \right\}$$

Substituting (2.14) and (2.12)₂ into (2.10)₂, the tangential inertial force becomes

$$F_{it} = e(\dot{\psi})^2 \frac{\rho R^3 L}{c} \left[\mathcal{A}_1 + \mathcal{A}_2 - \frac{12}{10} \frac{\varepsilon(8 + \varepsilon^2)}{(2 + \varepsilon^2)^2} \right] \tag{2.15}$$

Substituting (2.13) and (2.12)₁ into (2.10)₁, the radial inertia force becomes

$$F_{ir} = \frac{12\rho R^3 L \pi}{10c(\varepsilon^2 + 2)^2} \left[12 - 2 \frac{(10 - \varepsilon^2)(1 - \varepsilon^2)^{\frac{1}{2}}}{\varepsilon^2 + 2} \right] e(\dot{\psi})^2 \tag{2.16}$$

The oil film tangential force formula is obtained by adding tangential viscous force formula (2.6)₂ and tangential inertial force formula (2.15). The tangential force becomes

$$F_t = F_{it} + F_{tc} = e(\dot{\psi})^2 \frac{\rho R^3 L}{c} \left[\mathcal{A}_1 + \mathcal{A}_2 - \frac{12}{10} \frac{\varepsilon(8 + \varepsilon^2)}{(2 + \varepsilon^2)^2} \right] - \frac{\mu R^3 L}{c^3} \frac{12\pi}{(2 + \varepsilon^2)(1 - \varepsilon^2)^{\frac{1}{2}}} e\dot{\psi} \tag{2.17}$$

The equivalent oil film damping is

$$C = -\frac{F_t}{e(\dot{\psi})} = -\dot{\psi} \frac{\rho R^3 L}{c} \left[\mathcal{A}_1 - \mathcal{A}_2 + \frac{12}{10} \frac{\varepsilon(8 + \varepsilon^2)}{(2 + \varepsilon^2)^2} \right] + \frac{\mu R^3 L}{c^3} \frac{12\pi}{(2 + \varepsilon^2)(1 - \varepsilon^2)^{\frac{1}{2}}} \tag{2.18}$$

The oil film radial force formula is obtained by adding radial viscous force formula (2.6)₁ and radial inertial force formula (2.16). Then the radial force becomes

$$F_r = F_{ir} + F_{rc} = \frac{12\rho R^3 L \pi}{10c(\varepsilon^2 + 2)^2} \left[12 - 2 \frac{(10 - \varepsilon^2)(1 - \varepsilon^2)^{\frac{1}{2}}}{\varepsilon^2 + 2} \right] e(\dot{\psi})^2 - \frac{\mu R^3 L}{c^3} \frac{24\varepsilon}{(2 + \varepsilon^2)(1 - \varepsilon^2)} e\dot{\psi} \tag{2.19}$$

The equivalent oil film stiffness is

$$K = -\frac{F_r}{e} = -\frac{12\rho R^3 L \pi}{10c(\varepsilon^2 + 2)^2} \left[12 - 2 \frac{(10 - \varepsilon^2)(1 - \varepsilon^2)^{\frac{1}{2}}}{\varepsilon^2 + 2} \right] (\dot{\psi})^2 + \frac{\mu R^3 L}{c^3} \frac{24\varepsilon}{(2 + \varepsilon^2)(1 - \varepsilon^2)} \dot{\psi} \tag{2.20}$$

From the solution analysis of the above equation, it can be seen that the inertia force of the oil film fluid has a great influence on the oil film damping. When the journal speed is large, the influence of oil film inertia force should be considered in the analysis of the squeeze oil film force.

3. Numerical simulation verification and analysis

3.1. SFD solution model and numerical simulation verification

According to the geometry of SFD shown in Fig. 2, the fluid domain model can be established according to the parameters of SFD, as shown in Fig. 2a. It is considered a computational domain. The hexahedral mesh has been generated by the Multizone mesh generation method. The fluid domain model grid is shown in Fig. 2b. The model local mesh of the fluid domain is shown in Fig. 2c. According to the assumption of the Reynolds equation, the flow condition is usually regarded as laminar flow, which conforms to Newton's viscosity law (Crandall and El-Shafei, 1993). In the numerical simulation, the lubricating oil used in model 1 is ISO VG2 reference (Zhou *et al.*, 2020b), and the room temperature is 23°C. The dynamic viscosity of the oil is $\mu = 0.0031$ Pa·s and density $\rho = 785$ kg/m³. The lubricating oil used in model 2 is the mixture of ISO VG2 and Aviation No. 8 lubricating oil. Its dynamic viscosity is $\mu = 0.0035$ Pa·s, density $\rho = 850$ kg/m³. In order to verify the derived models, CFD software simulation is conducted on two different SFDs. Geometric parameters and lubricant properties are listed in Table 1 and 2.

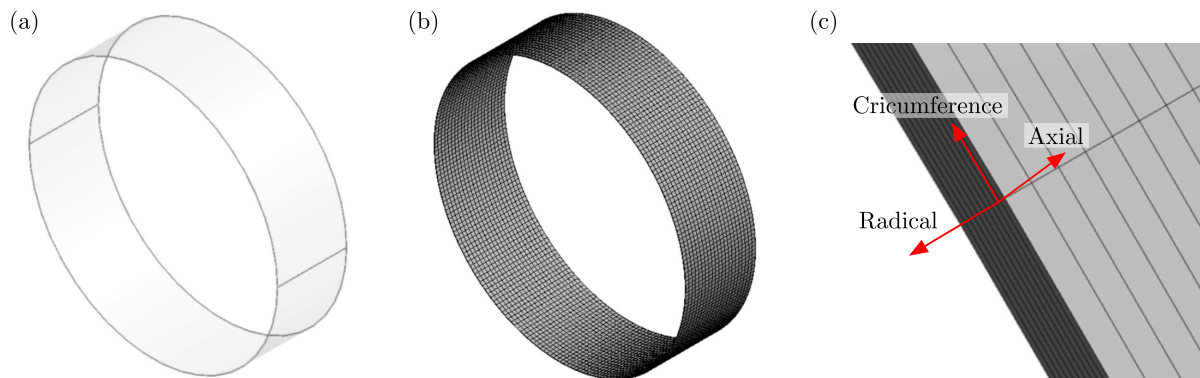


Fig. 2. 3D SFD model: (a) SFD model, (b) SFD meshing, (c) local mesh of fluid domain

Table 1. Theoretical model 1 geometric dimensions and lubricating oil parameters

Journal diameter D [mm]	Oil film clearance c [mm]	Axial length L [mm]	Density ρ [kg/m ³]	Dynamic viscosity μ [Pa·s]
73.8	0.14	20.6	785	0.0031

Table 2. Theoretical model 2 geometric dimensions and lubricating oil parameters

Journal diameter D [mm]	Oil film clearance c [mm]	Axial length L [mm]	Density ρ [kg/m ³]	Dynamic viscosity μ [Pa·s]
74.92	0.15	18.2	850	0.0035

According to reference (Zhou *et al.*, 2020a,b), the simulation is conducted on CFX. The grid division adopts the oil film axial grid of 0.06 mm, the oil film circumferential grid of 1 mm and the oil film radial grid of 10 layers. On the premise of considering both CFD simulation analysis accuracy and calculation time, this paper adopts the number of calculation cycles as 3 cycles, and the time step of each cycle takes 200 steps to obtain the convergent solution of the SFD oil film damping and stiffness.

Since the SFD Reynolds number is small, the flow state is set to a laminar flow. The boundary conditions are shown in Fig. 3. According to the LBA, the axial end of the “end land” is modeled as a wall to ambient pressure. The housing and journal of SFD is set to the “wall”. The housing is stationary, while the journal moves as circular centered-orbit motion in the steady state as follows (Zhou *et al.*, 2020a,b)

$$X = e \cos(\Omega t) \quad Y = e \sin(\Omega t) \quad (3.1)$$

where e is the eccentricity and Ω the precession speed. By changing e and Ω , different precession amplitudes and precession frequencies are simulated, and the conversion relationship between the precession speed and frequency is $\Omega = 2\pi f$.

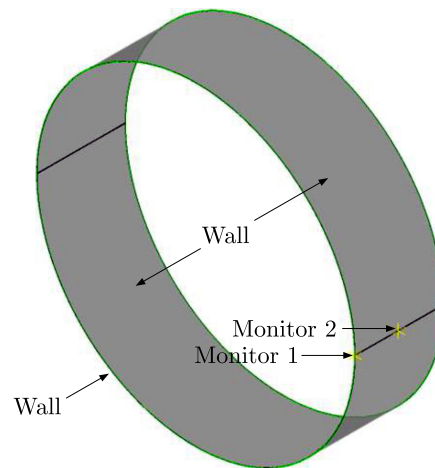


Fig. 3. SFD boundary conditions

In order to better observe the movement of the oil film, the monitoring point 1 and point 2 are added to observe the pressure change. The monitoring point 1 is located at the axial edge of the SFD, and the monitoring point 2 is located in the middle of the oil film, as shown in Fig. 3.

The tangential F_t and radial force F_r were obtained by integrating the oil film pressure obtained by numerical simulation, and then the corresponding oil film damping C and oil film stiffness K coefficients were obtained. The corresponding integral formula is shown in Eq. (3.2), where θ_1 and θ_2 represent the boundary of the oil film pressure zone

$$F_r = - \int_{L/2}^{L/2} \int_{\theta_1}^{\theta_2} P \cos(\theta) R d\theta dz \quad F_t = - \int_{L/2}^{L/2} \int_{\theta_1}^{\theta_2} P \sin(\theta) R d\theta dz \quad (3.2)$$

3.2. Analysis of the effect of eccentricity ratio on vibration reduction characteristics of the sealed ends SFD

In order to analyze the effect of journal eccentricity ratio on dynamic characteristics of the oil film, the oil film damping and stiffness are calculated by the theoretical formula and CFX simulation at a different eccentricity ratio of 100 Hz. The comparison results are shown in Figs. 4 and 5.

Through comparative analysis, it can be seen that the damping and stiffness of SFD with end seals roughly increase with an increase of the eccentricity ratio, but the increase range is small. Therefore, considering the oil film inertia is conducive to reduce the amplitude and improve the stability.

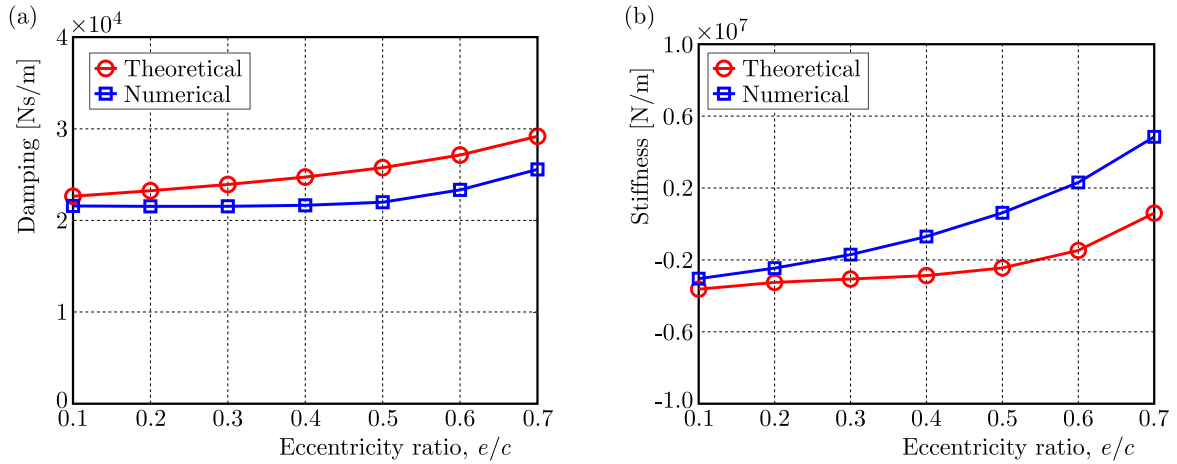


Fig. 4. Model 1 curve of (a) damping and (b) stiffness with eccentricity ratio

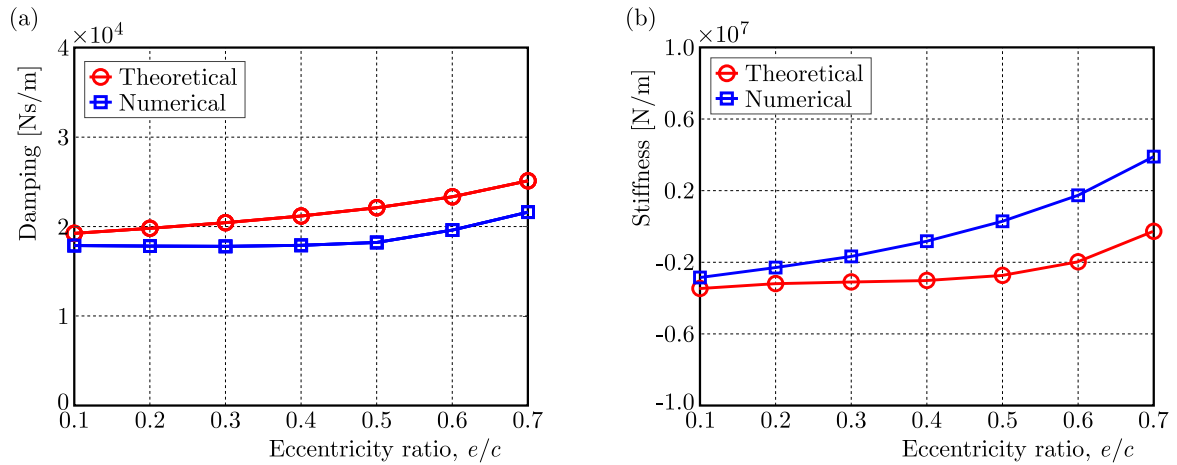


Fig. 5. Model 2 (a) damping and (b) stiffness curve with eccentricity ratio

4. Comparative analysis of sealed ends and open ends SFD

4.1. Numerical solution of short bearing SFD simulation

Referring to derivation of the theoretical formula of the short bearing SFD considering the inertia of the oil film, the oil film stiffness and equivalent oil film damping formula of the short bearing SFD containing the inertia term during stable circular precession are obtained (Zhou *et al.*, 2020a,b)

$$\begin{aligned}
 K &= \frac{\mu RL^3}{c^3} \left[\frac{2\varepsilon}{(1-\varepsilon^2)^2} \right] \omega - \frac{\pi \rho RL^3}{70c\varepsilon^2} \left[27 - \frac{27-17\varepsilon^2}{(1-\varepsilon^2)^{\frac{1}{2}}} \right] \omega^2 \\
 C &= \frac{\mu RL^3 \pi}{2c^3(1-\varepsilon^2)^{\frac{3}{2}}} - \frac{27\rho RL^3}{70c\varepsilon} \left(2 + \frac{1}{\varepsilon} \ln \frac{1-\varepsilon}{1+\varepsilon} \right) \omega
 \end{aligned} \tag{4.1}$$

In order to study the vibration reduction performance of the short open ends SFD, a numerical modeling of the short open ends SFD is firstly carried out. In order to compare the dynamic characteristics of the the sealed ends SFD and the the open ends SFD, the same geometric parameters and meshing are used to reduce the effect of the corresponding factors. Figure 6 shows the local oil film absolute pressure gradient distribution of the open ends SFD and the

sealed ends SFD when the eccentricity ratio is $\varepsilon = 0.1$ and the precession frequency $f = 50$ Hz, respectively.

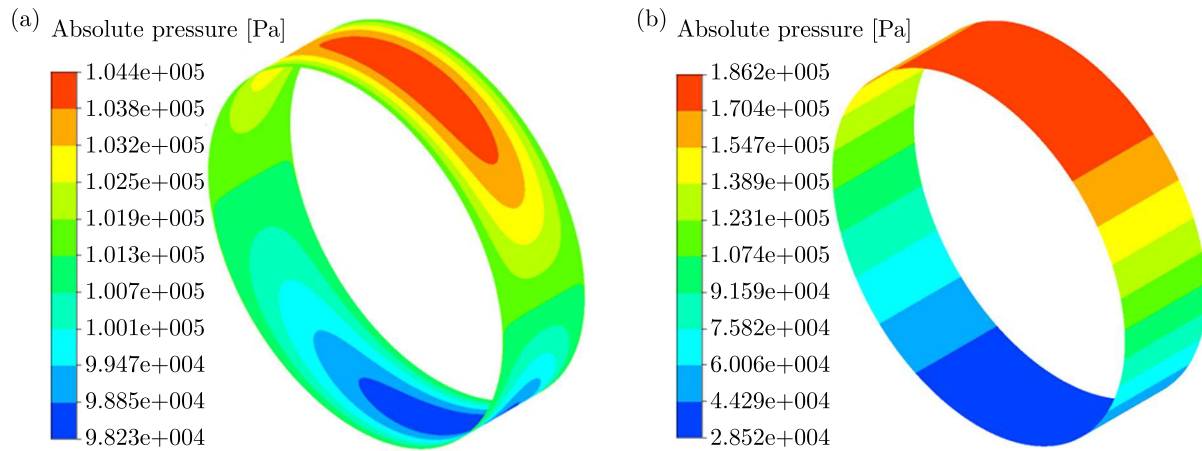


Fig. 6. SFD oil film pressure distribution: (a) open ends SFD oil film, (b) sealed ends SFD oil film

It can be seen from the pressure cloud diagram that because the short open ends SFD is open at both ends in the axial direction, and the oil film pressure change is mainly concentrated in the middle of the oil film, a certain gradient change from the middle to the two ends is observed, whereas the short sealed ends SFD is sealed at both ends in the axial direction. In the entire oil film area, there is a certain pressure gradient change. The oil film damping which plays an important role in vibration reduction is obtained by integrating the oil film pressure along the axial and circumferential directions to determine the tangential component of the oil film force. So it can be seen from the cloud diagram that the actual working oil film area of the short sealed ends SFD is larger than that of the short open ends SFD with the same structural size. Since the reference pressure at the axial ends of the short open ends SFD is the ambient pressure (0.1 MPa), the peak value of the oil film pressure under the same working conditions is also smaller than the short sealed ends SFD.

4.2. Comparative analysis of vibration reduction characteristics of the sealed and open ends SFD

The oil film tangential and radial forces are obtained by integrating the oil film pressure, and then the corresponding oil film damping and oil film stiffness are obtained. Taking the eccentricity ratio of $\varepsilon = 0.1$ and precession frequency f of 50 Hz, 75 Hz, 100 Hz, 125 Hz and 150 Hz as an example to compare damping and stiffness of the sealed and open ends SFD under the same structural parameters and working conditions, the theoretical results of model 1 are shown in Figs. 7 and 8, and the results of model 2 are shown in Figs. 9 and 10. Theoretical formula 1 is the LBA damping and stiffness formula with the inertia term, and numerical simulation 1 corresponds to the sealed ends SFD. Theoretical formula 2 is the SBA damping and stiffness formula with the inertia term, and numerical simulation 2 is made for the open ends SFD.

From the comparison curves Figs. 7-10, it can be seen that for both models 1 and 2, the variation laws of oil film damping and oil film stiffness obtained by CFD simulation with the precession frequency are in good agreement with the corresponding results obtained by the theoretical formula. With an increase of the precession frequency, the corresponding oil film damping of both sealed and open ends SFD shows an increasing trend, whereas the oil film stiffness shows a decreasing trend. Both the LBA and SBA damping and stiffness formula with the inertia term are obtained by logical simplification and assumption of oil film pressure and velocity, so there is a small deviation from the simulation results. Under the same working

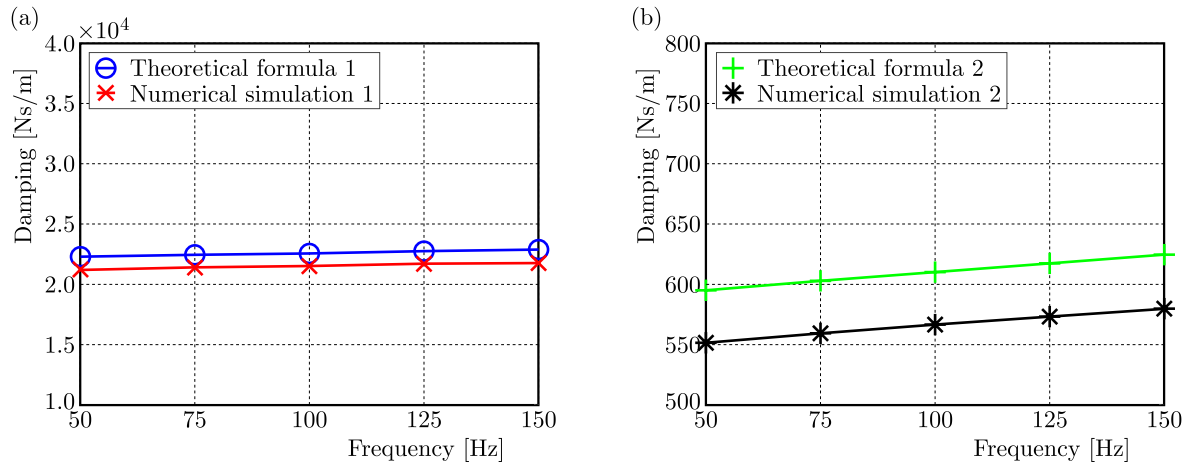


Fig. 7. Model 1 oil film damping comparison verification curve: (a) the sealed ends SFD damping versus frequency, (b) the open ends SFD damping versus frequency

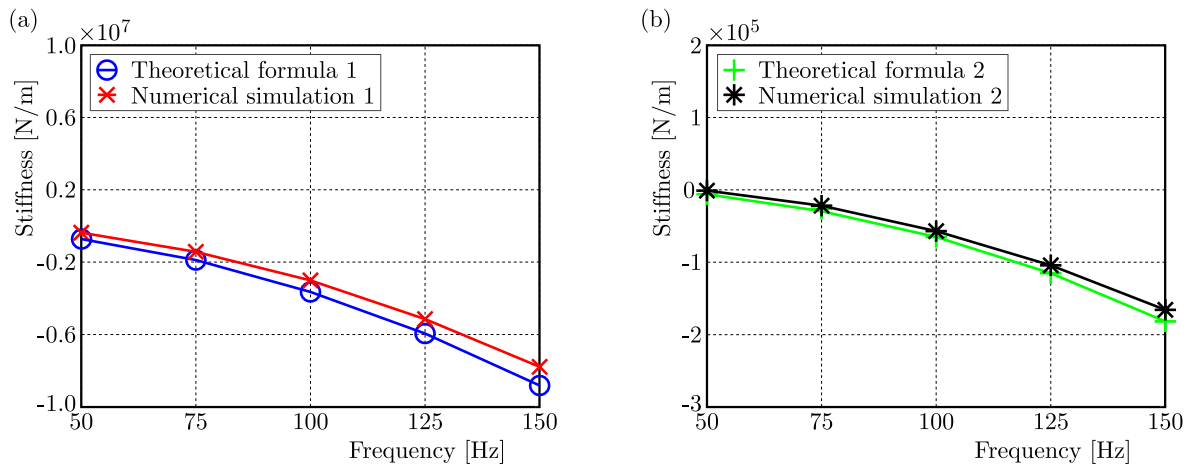


Fig. 8. Model 1 oil film stiffness comparison verification curve: (a) the sealed ends SFD damping versus frequency, (b) the open ends SFD damping versus frequency

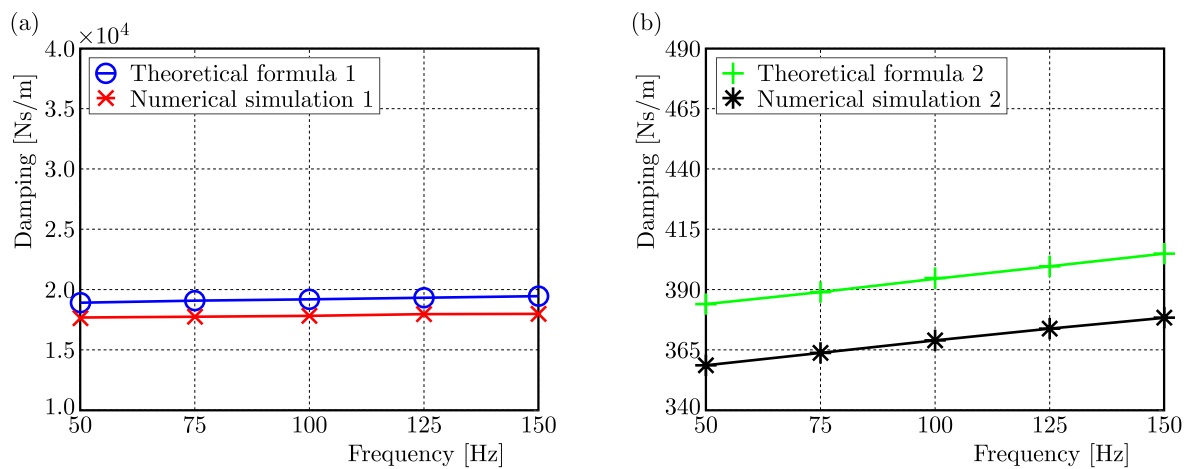


Fig. 9. Model 2 oil film damping comparison verification curve: (a) the sealed ends SFD damping versus frequency, (b) the open ends SFD damping versus frequency

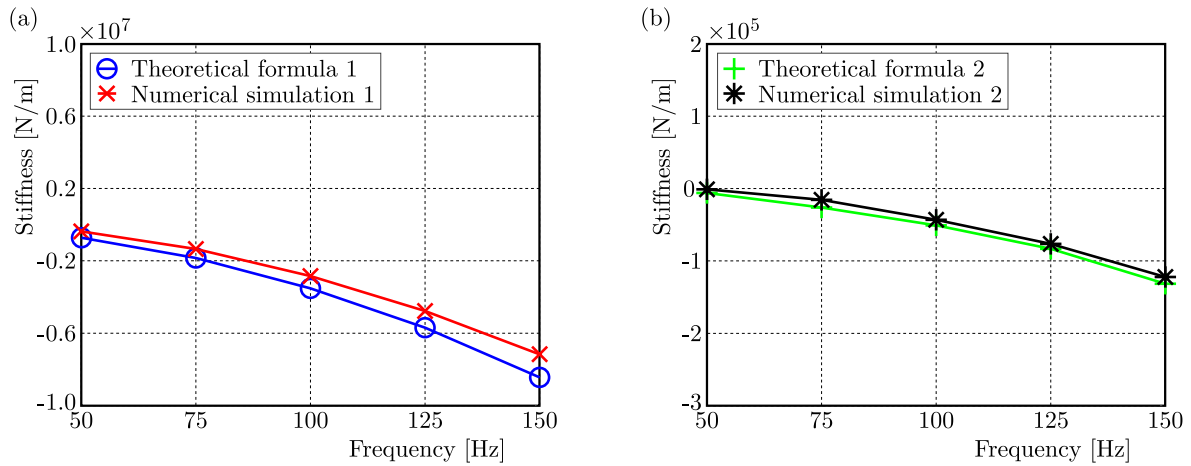


Fig. 10. Model 2 oil film stiffness comparison verification curve: (a) the sealed ends SFD damping versus frequency, (b) the open ends SFD damping versus frequency

conditions, the sealed ends SFD reveals characteristics of larger oil film damping and smaller oil film stiffness.

5. Conclusions

In this paper, an energy approximation method is used to deduce oil film damping and stiffness formulas of SFD under the assumption of long bearings. A numerical model of SFD under the LBA is established. The derived theoretical formulas are in good agreement with the numerical simulation results. The following conclusions are obtained through theoretical analysis and numerical simulation:

- The oil film damping and oil film stiffness of the sealed ends SFD generally tend to increase with a growth of the eccentricity ratio. The range of the increase of stiffness is small, which shows that the SFD with sealed ends SFD considering the effect of inertial force is conducive to reduce the amplitude and improve the stability.
- With an increase of the precession frequency of the sealed and open ends SFD, the oil film damping generally shows an increasing trend, and the oil film stiffness decreases.
- The variation laws of sealed and open ends SFD damping and stiffness obtained by CFD simulation with the precession frequency are in good agreement with the corresponding results obtained by the LBA and SBA theoretical formulas.
- Under the same working conditions and structural dimensions, the sealed ends SFD has greater oil film damping.

Acknowledgement

This research was supported by the National Natural Science Foundation of China (52175106); Plan for Young and Middle-aged Innovators of Shenyang (No: RC220326). The authors are grateful to the reviewers for their insightful and constructive comments.

References

1. BOOKER J., 1965, A table of the journal-bearing integral, *Journal of Basic Engineering*, **87**, 2, 533-535

2. CHEN X., REN G.M., GAN X.H., 2021. Dynamic behavior of a flexible rotor system with squeeze film damper considering oil-film inertia under base motions, *Nonlinear Dynamics*, **106**, 4, 3117-3145
3. CRANDALL S.H., EL-SHAFAEI A., 1993, Momentum and energy approximations for elementary squeeze-film damper flows, *Journal of Applied Mechanics*, **60**, 3, 728-736
4. DOUSTI S., GERAMI A., DOUSTI M., 2016, A numerical CFD analysis on supply groove effects in high pressure, open end squeeze film dampers, *International Journal of Engineering Innovation and Research*, **5**, 1, 80-89
5. EL-SHAFAEI A., 1991, Unbalance response of a Jeffcott rotor incorporating long squeeze film dampers, *Journal of Vibration and Acoustics*, **113**, 85-94
6. EL-SHAFAEI A., 1995, Modeling fluid inertia forces of short journal bearings for rotor dynamic applications, *Journal of Vibration and Acoustics*, **117**, 462-469
7. EL-SHAFAEI A., CRANDALL S., 1991, Fluid inertia forces in squeeze film dampers, *Proceedings of the ASME 1991 Design Technical Conferences. 13th Biennial Conference on Mechanical Vibration and Noise: Rotating Machinery and Vehicle Dynamics*, **35**, 219-228
8. GUO Z., HIRANO T., KIRK R.G., 2005, Application of CFD analysis for rotating machinery – Part I: Hydrodynamic, hydrostatic bearings and squeeze film damper, *Journal of Engineering for Gas Turbines and Power*, **127**, 2, 445-451
9. HAMZEHLOUIA S., BEHDINAN K., 2016, Squeeze film dampers executing small amplitude circular-centered orbits in high-speed turbomachinery, *International Journal of Aerospace Engineering*, **1**, 1-16
10. KUZMA D.C., 1968, Fluid inertia effects in squeeze films, *Applied Scientific Research*, **18**, 1, 15-20
11. LEE G.J., KIM J., STEEN T., 2017, Application of computational fluid dynamics simulation to squeeze film damper analysis, *Journal of Engineering for Gas Turbines and Power*, **139**, 10, 1-11
12. MIYACHI T., HOSHIYA S., SOFUE Y., MATSUKI M., TORISAKI T., 1979, Oil squeeze film dampers for reducing vibration of aircraft gas turbine engines, *Proceedings of the ASME 1979 International Gas Turbine Conference and Exhibit and Solar Energy Conference. Volume 1B: Gas Turbines*, American Society of Mechanical Engineers, 1-11
13. SAN ANDRÉS L., SESHAGIRI S., 2013, Damping and inertia coefficients for two end sealed squeeze film dampers with a central groove: measurements and predictions, *Journal of Engineering for Gas Turbines and Power*, **135**, 11, 1-9
14. SAN ANDRÉS L., VANCE J.M., 1988, Effect of fluid inertia on the performance of squeeze film damper supported rotors, *Journal of Engineering for Gas Turbines and Power*, **110**, 1, 51-57
15. SZERI A.Z., 1980, *Fluid Film Lubrication*, Cambridge University Press, New York, USA
16. SZERI A.Z., RAIMONDI A.A., GIRON-DUARTE A., 1982, Linear force coefficients for squeeze film dampers, *Journal of Lubrication Technology*, **105**, 326-334
17. ZHOU H.L., CHEN X., ZHANG C.S., 2020a, Numerical simulation and influence factors analysis for dynamic characteristics of squeeze film damper, *Journal of Vibroengineering*, **22**, 7, 1593-1605
18. ZHOU H.L., CHEN X., ZHANG Y.Q., AI Y.T., SUN D., 2020b, An analysis on the influence of air ingestion on vibration damping properties of squeeze film dampers, *Tribology International*, **145**, 106168